

# Floquet engineering of low-energy dispersions and dynamical localization in a periodically kicked pseudospin-1 system

Lakpa Tamang\*, Tanay Nag<sup>†‡,\*</sup> and Tutul Biswas<sup>†</sup>

<sup>\*</sup>*Department of Physics, University of North Bengal,  
Raja Rammohunpur-734013, India*

<sup>†</sup>*SISSA, via Bonomea 265, 34136 Trieste, Italy*

<sup>‡</sup>*Institut für Theorie der Statistischen Physik,  
RWTH Aachen University, 52056 Aachen, Germany*

(Dated: December 22, 2024)

Much having learned about Floquet dynamics of pseudospin-1/2 system namely, graphene, we here address the stroboscopic properties of a periodically kicked pseudospin-1 fermionic system such as dice lattice that is alternatively known as  $T_3$  lattice. Likewise graphene, we reveal that one can, in principle, engineer various type of low energy dispersions around some specific points in the Brillouin zone by tuning the kicking parameter in the Hamiltonian along a particular direction. Our analytical analysis shows that one can experience different quasi-energy dispersions for example, Dirac type, semi-Dirac type, gapless line, absolute flat quasi-energy bands, depending on the specific values of the kicking parameter. Moreover, we numerically study the dynamics of a wave packet in this system; the quasi-energy dispersion allows us to understand the instantaneous structure of wave-packet at stroboscopic times. We find a situation where absolute flat quasi-energy bands lead to a complete dynamical localization of the wavepacket.

## I. INTRODUCTION

Graphene[1], a strictly two dimensional sheet of carbon atoms arranged on a honeycomb lattice, brings a new revolution in condensed matter physics due to its fascinating physical properties [2–4] and its potential application in the field of nanotechnology[5]. The itinerant electrons in graphene behave like quasiparticles of which the low energy massless excitations are described by the pseudospin-1/2 Dirac-Weyl equation. Thus, graphene provides a platform to study the fingerprints of the Dirac physics in realistic systems.

There exists an analogous model with  $T_3$ -symmetry, known as the dice lattice model[6 and 7], which also exhibits low energy massless excitations. The geometry of the dice lattice consists of an additional site being located at the center of each hexagon of the honeycomb lattice and that additional site is connected to one of the two inequivalent sites of the honeycomb lattice. A dice lattice can be found in a trilayer structure[8] of cubic lattices, namely,  $\text{SrTiO}_3/\text{SrIrO}_3/\text{SrTiO}_3$  grown in (111)-direction. It is also proposed that one can realize a dice lattice model in an optical lattice[9] by confining cold atoms using three pairs of counter propagating laser beams. A slightly modified lattice, named as,  $\alpha$ - $T_3$  lattice[10] is also an important topic of current research as it plays a role of interpolating between graphene and dice lattice through the variation of the parameter  $\alpha \in [0, 1]$  and this variation is associated with distinct non-trivial Berry phase. In recent years, a number of studies have been performed in dice and  $\alpha$ - $T_3$  lattice from the point of view of wide aspects such as topological localization[6 and 7], magnetic frustration[11 and 12], spin-orbit interaction induced phenomena[13], Klein tunneling[14 and 15], plasmon[16 and 17], magneto-optical conductivity[18–20], magnetotransport[21], spatial modulation effect[22], zitterbewegung[23], non-linear optical response[24], RKKY interaction[25 and 26], minimal conductivity[27], topological phases in a Haldane-dice lattice model[28] etc.

Although both graphene and dice lattice share same zero field spectrum nevertheless these two systems are fundamentally different. In graphene the pseudospin of a quasiparticle is  $S = 1/2$  whereas the dice lattice hosts quasiparticles with pseudospin  $S = 1$ . In an external magnetic field, graphene behaves like a diamagnet[29] while a dice lattice model exhibits paramagnetic[10] response. The Hall quantization[18 and 21] rules are also different in these two systems. The quasiparticles in graphene acquire a non-trivial Berry phase of  $\pi$  while traversing a closed loop around a high symmetry point in momentum space. In contrary, the quasiparticles in a dice lattice model do not pick any Berry phase during such movement.

Recent years have witnessed a tremendous quest to understand the microscopic details of quantum systems driven by external time periodic fields. The Floquet theory[30 and 31] provides an extremely useful theoretical framework to deal with the time periodic Hamiltonians corresponding to the driven systems. The studies[32–35] on graphene irradiated by the circularly polarized time periodic fields have become so impactful that an exciting research field of “Floquet topological insulators” has been emerged subsequently[36–38]. Over a period of last ten years, Floquet irradiated quantum systems have been explored extensively in the context of Floquet generation of strongly correlated phases[39–43] and symmetry protected topological phases[44–48, and 94] in many-body quantum systems, topological classification[49–57], symmetry breaking[58–65], Floquet-Majorana modes[66–71], topologically protected edge states[72–76] and Floquet topological phase transition[77 and 78], Floquet flat band [79]. It is worthy to mention that many of these phenomena have been realized experimentally[80–84] in recent past.

To study the stroboscopic properties of a driven quantum system, driving protocols like the  $\delta$ -function kicks, periodic in time, may be adopted. The impact of such driving protocol has far reaching consequences. This type of driving has been used to study a wide range of spectacular phenomena including non-equilibrium phase transition in a Dicke Model[85], local-

ization effect in a chain of hard core bosons[86], semimetallic phases in Harper models[87], edge modes in quantum Hall systems[88], low energy band engineering in graphene[89], Majorana edge mode in one dimensional systems[90] as well as in Kitaev model[91] on a honeycomb lattice, topological properties of Chern insulator[92], topological phase transition in Haldane-Chern insulator[93], generation of higher order topological insulator from a lower order topological insulating phase [94] and many more. Another interesting effect of periodic  $\delta$ -function driving on the quantum systems is to achieve dynamical localization of the quasiparticles. A number of systems like classical and quantum rotors[95–97], two level system[98], the Kapitza pendulum[99 and 100], bosons in optical lattice[101], linear chain of hard core bosons[86], graphene[89] etc exhibit dynamical localization phenomenon under periodic driving.

Given this background, one can comment that the study of Floquet dynamics in the three level system has not been addressed in great detail as it is investigated for two level systems. The transport properties of three level system can become significantly different from that of the former system hosts flat band. This also motivates us to investigate the three level dice model with pseudospin-1 that has the potential to exhibit intriguing band dispersions eventually leading to unusual non-equilibrium transport properties. In particular, we study the stroboscopic non-equilibrium properties of a periodically kicked dice lattice. We check that the character of the zero-energy flat band remains unaltered in presence of the  $\delta$ -function kicks. It is revealed that various types of low energy dispersions including Dirac type, semi-Dirac type, gapless line, absolute flat quasi-energy bands can be engineered around some special points in the Brillouin zone. This wide variety of dispersions entirely depends on the tuning of the kicking parameter and direction of periodic kicking. In addition, we study wave packet dynamics in this system. The periodic  $\delta$ -driving along the transverse direction causes the dynamical localization of the electronic wave packet corresponding to a certain strength of kicking parameter. The origin of this dynamical localization lies in the fact that all three quasi-energy bands become absolutely flat at certain kicking strength. For kicking in other directions, we obtain diffusive character of the wavepacket as we do not encounter a situation where all the three quasi-energy bands become flat.

This article is presented in the following way. In section II, we provide a brief description of the geometry and energy spectrum of the dice lattice. Detailed characteristics of the quasienergy spectrum of a periodically kicked dice lattice corresponding to different kicking schemes are described in section III. Different aspects of the wavepacket dynamics are investigated in section IV. Finally, we conclude our findings in section V.

## II. A DESCRIPTION OF THE DICE LATTICE

A dice lattice has a bipartite honeycomb like structure with an additional site at the center of each hexagon. As shown in

Fig. 1,  $A$  and  $B$  atoms form the honeycomb structure with nearest neighbor hopping amplitude  $t$ . The  $C$  atom sitting at the center of each hexagon is connected to the  $B$  atoms with hopping parameter  $t$ . Note that  $A$  and  $C$  atoms both are connected to the three  $B$  atoms, hence both have coordination number 3, named as rim sites. The  $B$  atom has the coordination number 6, known as hub site. Note that each nearest neighbor pair consists of one hub atom and one rim atom. Each unit cell contains three lattice sites. The lattice translational vectors are  $\mathbf{a}_1 = (\sqrt{3}a_0/2, 3a_0/2)$  and  $\mathbf{a}_2 = (-\sqrt{3}a_0/2, 3a_0/2)$ . Therefore the entire lattice is spanned by  $\mathbf{n} = n_1\mathbf{a}_1 + n_2\mathbf{a}_2$ ,  $n_1, n_2 \in \mathbb{Z}$ . The coordinates of  $A$  sites surrounded by the  $B$  site are  $\delta_A^1 = (0, -a_0)$ ,  $\delta_A^2 = \delta_A^1 + \mathbf{a}_1$ , and  $\delta_A^3 = \delta_A^1 + \mathbf{a}_2$ . The coordinates of  $C$  sites surrounded by the  $B$  site are  $\delta_C^i = -\delta_A^i$ ,  $i = 1, 2, 3$ . The reciprocal lattice vectors are  $\mathbf{b}_1 = b_0(1/\sqrt{3}, 1/3)$  and  $\mathbf{b}_2 = b_0(-1/\sqrt{3}, 1/3)$ , where  $b_0 = 2\pi/a_0$ .

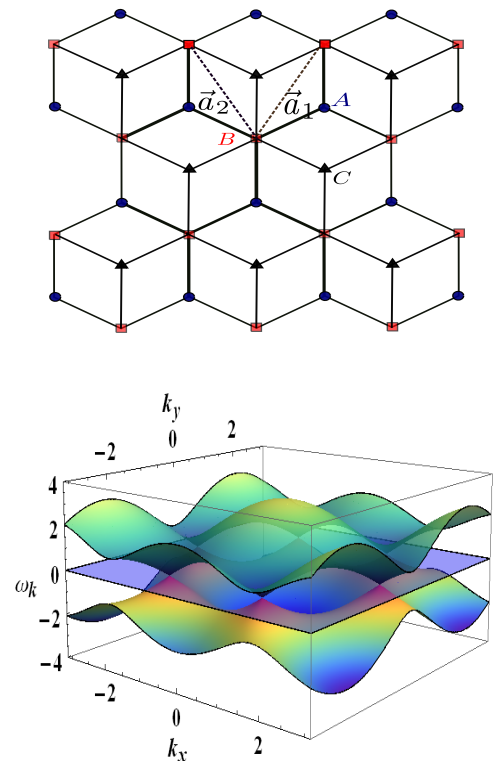


FIG. 1. In the upper panel the geometrical structure of a dice lattice is shown. The energy spectrum is given in the lower panel obtained from Eq.(3)

The nearest neighbor tight-binding Hamiltonian can be written as

$$H = -\gamma \sum_{\mathbf{n}, \delta_A} \left( b_{\mathbf{n}}^\dagger a_{\mathbf{n}+\delta_A} + a_{\mathbf{n}+\delta_A}^\dagger b_{\mathbf{n}} \right) - \gamma \sum_{\mathbf{n}, \delta_C} \left( b_{\mathbf{n}}^\dagger c_{\mathbf{n}+\delta_C} + c_{\mathbf{n}+\delta_C}^\dagger b_{\mathbf{n}} \right), \quad (1)$$

where  $\gamma$  is nearest neighbor hopping parameter. Here,  $a(a^\dagger)$ ,  $b(b^\dagger)$ , and  $c(c^\dagger)$  are the annihilation(creation) operators for the

sites  $A$ ,  $B$ , and  $C$ , respectively. Using the appropriate Fourier transformations the Hamiltonian in momentum space can be obtained as

$$H_{\mathbf{k}} = \frac{1}{\sqrt{2}} \begin{pmatrix} 0 & f_{\mathbf{k}} & 0 \\ f_{\mathbf{k}}^* & 0 & f_{\mathbf{k}} \\ 0 & f_{\mathbf{k}}^* & 0 \end{pmatrix} \quad (2)$$

with  $f_{\mathbf{k}} = -\gamma(1 + e^{-i\mathbf{k} \cdot \mathbf{a}_1} + e^{-i\mathbf{k} \cdot \mathbf{a}_2})$ . Note that the hopping parameter  $\gamma$  is rescaled with  $\gamma/\sqrt{2}$ . Diagonalizing  $H_{\mathbf{k}}$ , one can obtain the energy spectrum as  $\varepsilon_{\mathbf{k}}^{\pm} = \pm\omega_{\mathbf{k}}$  and  $\varepsilon_{\mathbf{k}}^0 = 0$ , where  $\omega_{\mathbf{k}}$  is given by

$$\omega_{\mathbf{k}} = \gamma \left[ 3 + 2 \cos(\sqrt{3}a_0k_x) + 4 \cos\left(\frac{\sqrt{3}}{2}a_0k_x\right) \cos\left(\frac{3}{2}a_0k_y\right) \right]^{\frac{1}{2}}. \quad (3)$$

Here, we have chosen  $\hbar = 1$  and henceforth this choice will be maintained throughout this article.

### III. QUASIENERGY DISPERSION OF A KICKED DICE LATTICE

Here, we discuss the situation when the system is subjected to time periodic  $\delta$ -kicks of period  $T$  in  $x$ ,  $y$ , and  $z$ -directions with strengths  $\alpha_x$ ,  $\alpha_y$ , and  $\alpha_z$ , respectively. This kicking process is described by the following Hamiltonian

$$V(t) = \sum_{\nu=x,y,z} \alpha_{\nu} S_{\nu} \sum_{m=-\infty}^{\infty} \delta(t - mT), \quad (4)$$

where  $S_{\nu}$  ( $\nu = x, y, z$ ) are the components of the usual spin operator  $S = 1$ , namely,

$$S_x = \frac{1}{\sqrt{2}} \begin{pmatrix} 0 & 1 & 0 \\ 1 & 0 & 1 \\ 0 & 1 & 0 \end{pmatrix}, \quad S_y = \frac{1}{\sqrt{2}} \begin{pmatrix} 0 & -i & 0 \\ i & 0 & -i \\ 0 & i & 0 \end{pmatrix},$$

$$S_z = \begin{pmatrix} 1 & 0 & 0 \\ 0 & 0 & 0 \\ 0 & 0 & -1 \end{pmatrix}. \quad (5)$$

It is assumed that all the unit cells are being subjected to equal driving. We are mainly interested in the stroboscopic behavior of the system measured at the end of each driving period. The Floquet theory would thus be the best tool to handle the situation. The Floquet operator  $U_F(T)$  describing the time evolution of the quantum states through one period  $T$  is given by  $U_F(T) = e^{-i\alpha \cdot S} e^{-iH_{\mathbf{k}}T}$ . According to the Floquet theorem, the energy eigenvalues of  $U_F(T)$  are  $e^{\pm i\Delta_{\mathbf{k}}T}$ , where  $\Delta_{\mathbf{k}}$  is known as the quasienergy. It is too cumbersome to compute the quasienergies by considering all the kicking simultaneously. Therefore, we will consider cases of individual kicking separately.

#### A. X-Kicking

With the particular choice of kicking parameter, namely,  $\alpha_x \neq 0$ ,  $\alpha_y = 0$ , and  $\alpha_z = 0$ , the Floquet operator becomes  $U_F^x(T) = e^{-i\alpha_x S_x} e^{-iH_{\mathbf{k}}T}$ . The eigenvalues of  $U_F^x(T)$  can be obtained in a straightforward manner in order to calculate the corresponding quasienergy  $\Delta_{\mathbf{k}}$  (See Appendix for a detailed derivation). Now the Floquet operator can be written in the following matrix form as

$$U_F^x(T) = \begin{pmatrix} A & -iB^* & C^* \\ -iP & Q & -iP^* \\ C & -iB & A^* \end{pmatrix}, \quad (6)$$

where

$$\begin{aligned} A &= pa - qb + rc \\ B &= pb + q(2a - 1) + rb^* \\ C &= pc - qb + ra \\ P &= (2p - 1)b + q(a + c) \\ Q &= (2p - 1)(2a - 1) - q(b + b^*). \end{aligned}$$

with

$$\begin{aligned} p &= \frac{1}{2}(1 + \cos \alpha_x), \quad q = \frac{1}{\sqrt{2}} \sin \alpha_x, \\ r &= \frac{1}{2}(-1 + \cos \alpha_x), \quad a = \frac{1}{2}[1 + \cos(\omega_{\mathbf{k}}T)], \\ b &= \frac{1}{\sqrt{2}} e^{-i\theta_{\mathbf{k}}} \sin(\omega_{\mathbf{k}}T), \quad c = \frac{1}{2} e^{-2i\theta_{\mathbf{k}}} [1 + \cos(\omega_{\mathbf{k}}T)]. \end{aligned}$$

Here, the angle  $\theta_{\mathbf{k}}$  is defined in a way such that  $f_{\mathbf{k}} = \omega_{\mathbf{k}} e^{i\theta_{\mathbf{k}}}$ . The eigen values of  $U_F^x(T)$  are obtained as  $\lambda^0 = 1$  and  $\lambda_{\pm} = \kappa^x \pm i\sqrt{1 - (\kappa^x)^2}$  which consequently give corresponding quasienergies

$$\Delta_{\mathbf{k}}^0 = 0, \quad \Delta_{\mathbf{k}}^{\pm} = \pm\Delta_{\mathbf{k}} = \pm\frac{1}{T} \cos^{-1}(\kappa^x), \quad (7)$$

where

$$\begin{aligned} \kappa^x &= \frac{1}{2} \left( \cos \alpha_x - 1 \right) \sin^2 \theta_{\mathbf{k}} - \sin \alpha_x \cos \theta_{\mathbf{k}} \sin(\omega_{\mathbf{k}}T) \\ &+ \frac{1}{2} \left[ \sin^2 \theta_{\mathbf{k}} + \cos \alpha_x (1 + \cos^2 \theta_{\mathbf{k}}) \right] \cos(\omega_{\mathbf{k}}T). \end{aligned} \quad (8)$$

It is noteworthy that the quasi-energy spectrum contains one flat band and two dispersive bands. In other words, we may say that the fate of the zero energy flat band of the un-kicked system remains unaltered. Similar feature is also obtained for a dice lattice illuminated by circularly polarized radiation in the terahertz regime[65]. Nevertheless, the external kicking modifies the characters of the dispersive bands significantly.

To analyze the characteristics of the quasi-energy spectrum let us begin by writing  $f_{\mathbf{k}}$  as  $f_{\mathbf{k}} = -\gamma(\xi_{\mathbf{k}} - i\delta_{\mathbf{k}})$  which enable us to express  $\cos \theta_{\mathbf{k}}$  and  $\sin \theta_{\mathbf{k}}$  as:  $\cos \theta_{\mathbf{k}} = -\gamma\xi_{\mathbf{k}}/\omega_{\mathbf{k}}$  and  $\sin \theta_{\mathbf{k}} = \gamma\delta_{\mathbf{k}}/\omega_{\mathbf{k}}$  with  $\omega_{\mathbf{k}} = \sqrt{\xi_{\mathbf{k}}^2 + \delta_{\mathbf{k}}^2}$ . Here,

$$\begin{aligned} \xi_{\mathbf{k}} &= 1 + 2 \cos\left(\frac{\sqrt{3}k_x a}{2}\right) \cos\left(\frac{3k_y a}{2}\right) \\ \delta_{\mathbf{k}} &= 2 \cos\left(\frac{\sqrt{3}k_x a}{2}\right) \sin\left(\frac{3k_y a}{2}\right). \end{aligned} \quad (9)$$

At gapless points  $\kappa^x$  should be unity so that  $\Delta_k^\pm = 0$ . This will be possible only when the following conditions are satisfied simultaneously:  $\sin \theta_k = 0$ ,  $\cos \theta_k = -1$ , and  $\alpha_x = \omega_k T$ .

Therefore, for the gapless points  $(k_x^0, k_y^0)$  we have the following conditions

$$\begin{aligned} 1 + 2 \cos \left( \frac{\sqrt{3}k_x^0 a}{2} \right) \cos \left( \frac{3k_y^0 a}{2} \right) &= \frac{\alpha_x}{\gamma T} \\ \cos \left( \frac{\sqrt{3}k_x^0 a}{2} \right) \sin \left( \frac{3k_y^0 a}{2} \right) &= 0 \end{aligned} \quad (10)$$

which further give

$$\begin{aligned} \cos \left( \frac{\sqrt{3}k_x^0 a}{2} \right) &= \frac{1}{2} \left( \frac{\alpha_x}{\gamma T} - 1 \right) \\ \sin \left( \frac{3k_y^0 a}{2} \right) &= 0. \end{aligned} \quad (11)$$

It is worthy to note that the value of  $\alpha_x$  must lie in between  $-\gamma T$  and  $3\gamma T$  in order to obtain gapless points. To see how the quasienergy spectrum behaves around the gapless points  $(k_x^0, k_y^0)$ , we approximate  $\cos \theta_k$  and  $\sin \theta_k$  as:  $\cos \theta_k \approx -[1 - \delta_k^2/(2\xi_k^2)]$  and  $\sin \theta_k \approx \delta_k/\xi_k$ . With this approximation we obtain following equation for the quasienergy spectrum

$$\begin{aligned} \cos(\Delta_k^x T) &= \left( 1 - \frac{\delta_k^2}{2\xi_k^2} \right) \cos(\omega_k T - \alpha_x) \\ &+ \frac{\delta_k^2}{2\xi_k^2} [\cos(\omega_k T) + (\cos \alpha_x - 1)]. \end{aligned} \quad (12)$$

Expanding the sine and cosine functions about the gapless point, we get

$$(\Delta_k^x T)^2 = (\omega_k T - \alpha_x)^2 + \frac{2\delta_k^2}{\xi_k^2} (1 - \cos \alpha_x). \quad (13)$$

In the vicinity of the gapless points, we set  $\xi_k = \alpha_x/(\gamma T)$  to obtain the velocity components of the quasi-particle

$$\begin{aligned} v_x &= -\frac{\sqrt{3}a}{2T} \sqrt{3\gamma^2 T^2 + 2\gamma T \alpha_x - \alpha_x^2} \\ v_y &= \frac{3a}{T} \frac{(\alpha_x - \gamma T)}{\alpha_x} \sin \left( \frac{\alpha_x}{2} \right). \end{aligned} \quad (14)$$

Note that the velocity along  $y$ -direction vanishes for  $\alpha_x = \gamma T$ . This feature indicates that the quasi-energy spectrum around the gapless point should be linear along  $k_x$ -direction. Let us understand this argument quantitatively. In this particular case, the gapless conditions reduce to  $\sin(3ak_y^0/2) = 0$  and  $\cos(\sqrt{3}ak_x^0/2) = 0$  which give gapless point  $(k_x^0, k_y^0) = (\pi/(\sqrt{3}a), 0)$ . We find that near  $(k_x^0, k_y^0)$  the quasienergy spectrum behaves as

$$\begin{aligned} \Delta_k^x &= \gamma(\sqrt{3}k_x a - \pi - 2), \quad \text{for } k_y = 0, \\ \Delta_k^x &= 0, \quad \text{for } k_x = \frac{\pi}{\sqrt{3}a}. \end{aligned} \quad (15)$$

Therefore, the quasi-energy spectrum becomes gapless along the line  $k_x = \pi/(\sqrt{3}a)$ . In Fig. 2(a), we plot the exact quasi-energy spectrum [Eq.(7)] for  $\alpha_x = \gamma T$ . This figure also supports our arguments given above.

There exists another interesting case corresponding to  $\alpha_x = 3\gamma T$ . Here, the gapless conditions will be determined by  $\sin(3ak_y^0/2) = 0$  and  $\cos(\sqrt{3}ak_x^0/2) = 1$  which implies the gapless point  $(k_x^0, k_y^0) = (0, 0)$ . This is known as merging of Dirac points, achieved by the application of periodic  $\delta$ -kicking. Similar phenomenon has been revealed in the case of graphene[77 and 89] also. Near  $(k_x^0, k_y^0)$  the quasienergy spectrum exhibits the following features

$$\begin{aligned} \Delta_k^x &= \frac{2a}{T} \sin \left( \frac{3\gamma T}{2} \right) k_y, \quad \text{for } k_x = 0, \\ \Delta_k^x &= 3\gamma T a^2 k_x^2, \quad \text{for } k_y = 0. \end{aligned} \quad (16)$$

Thus the quasi-energy spectrum exhibits semi-Dirac dispersion which is Dirac like along  $k_y$  and quadratic along  $k_x$ . This interesting feature is also depicted in Fig. 2(b) which is obtained by plotting the exact quasi-energy spectrum [Eq.(7)] for  $\alpha_x = 3\gamma T$ .

## B. Y-Kicking

The Floquet operator in this case is reduced to  $U_F^y(T) = e^{-i\alpha_y S_y} e^{-iH_k T}$  which will take the following explicit form

$$U_F^y(T) = \begin{pmatrix} A' & B'^* & C'^* \\ -iP' & Q' & P'^* \\ C' & -B' & A'^* \end{pmatrix}, \quad (17)$$

where

$$\begin{aligned} A' &= p'a + iq'b + r'c \\ B' &= ip'b - q'(2a - 1) + ir'b^* \\ C' &= p'c - iq'b + r'a \\ P' &= i(2p' - 1)b - q'(a - c) \\ Q' &= (2p' - 1)(2a - 1) + iq'(b - b^*) \end{aligned}$$

along with  $p' = (1 + \cos \alpha_y)/2$ ,  $q = \sin \alpha_y/\sqrt{2}$ , and  $r = (1 - \cos \alpha_y)/2$ .

In this case the quasi-energies are obtained as

$$\Delta_k^{y0} = 0, \quad \Delta_k^{y\pm} = \pm \Delta_k^y = \pm \frac{1}{T} \cos^{-1}(-\kappa^y) \quad (18)$$

where

$$\begin{aligned} \kappa^y &= \frac{1}{2} \left( 1 - \cos \alpha_y \right) \cos^2 \theta_k - \sin \alpha_y \sin \theta_k \sin(\omega_k T) \\ &- \frac{1}{2} \left[ \cos^2 \theta_k + \cos \alpha_y (1 + \sin^2 \theta_k) \right] \cos(\omega_k T). \end{aligned} \quad (19)$$

Let us now find the  $k$ -points at which the quasienergy spectrum becomes gapless. In order to have  $\Delta_k^y = 0$ , we need  $\kappa^y = -1$ . This criterion will be fulfilled by the following choices:  $\cos \theta_k = 0$ ,  $\sin \theta_k = 1$ , and  $\alpha_y = \omega_k T$ . Therefore, at the gapless points  $\xi_k$  vanishes. This leads to infer that the



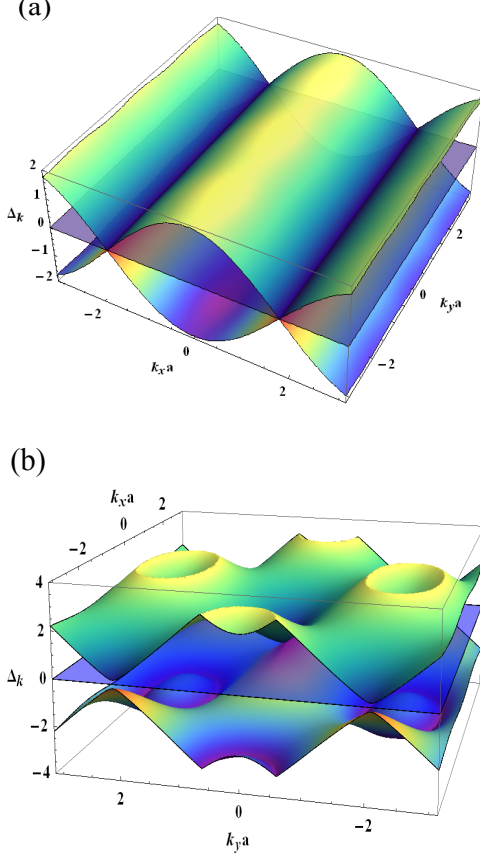


FIG. 2. Sketch of the quasi-energy spectrum corresponding to periodic kicking along  $X$ -direction for (a)  $\alpha_x = \gamma T$  and (b)  $\alpha_x = 3\gamma T$ . For,  $\alpha_x = \gamma T$ , the spectrum exhibits a gapless line at  $k_x = \pi/(\sqrt{3}a)$  along  $k_y$ -direction and a linear dispersion along  $k_x$ -direction around the gapless line as described in Eq.(15). For  $\alpha_x = 3\gamma T$ , the spectrum exhibits semi-Dirac dispersion, linear along  $k_y$  and quadratic along  $k_x$  as obtained in Eq.(16).

following conditions would be satisfied by the gapless point  $(k_x^0, k_y^0)$  simultaneously:

$$\begin{aligned} \cos\left(\frac{\sqrt{3}ak_x^0}{2}\right) &= \frac{\sqrt{\alpha_y^2 + \gamma^2 T^2}}{2\gamma T}, \\ \sin\left(\frac{3ak_y^0}{2}\right) &= \frac{\alpha_y}{\sqrt{\alpha_y^2 + \gamma^2 T^2}}, \\ \cos\left(\frac{3ak_y^0}{2}\right) &= -\frac{\gamma T}{\sqrt{\alpha_y^2 + \gamma^2 T^2}}. \end{aligned} \quad (20)$$

Note that, in this case the upper bound of  $\alpha_y$  is  $\alpha_y \leq \sqrt{3}\gamma T$ .

We now proceed to calculate effective quasienergy spectrum in the vicinity of the gapless points. Here, we consider the following approximations:  $\sin \theta_k \approx [1 - \xi_k^2/(2\delta_k^2)]$  and  $\cos \theta_k \approx -\xi_k/\delta_k$ . The equation for quasienergy takes the

form

$$\begin{aligned} \cos(\Delta_k^y T) &= \left(1 - \frac{\xi_k^2}{2\delta_k^2}\right) \cos(\omega_k T - \alpha_y) \\ &+ \frac{\xi_k^2}{2\delta_k^2} [\cos(\omega_k T) + (\cos \alpha_y - 1)]. \end{aligned} \quad (21)$$

Expanding the cosine functions near the gapless point, we get

$$(\Delta_k^y T)^2 = (\omega_k T - \alpha_y)^2 + \frac{2\xi_k^2}{\delta_k^2} (1 - \cos \alpha_y). \quad (22)$$

By considering  $\delta_k = \alpha_y/(\gamma T)$  at the gapless points, we obtain the velocity components of the quasiparticle as

$$\begin{aligned} v_x &= \frac{\sqrt{3}a}{2T} \left[ \frac{4\gamma T}{\alpha_y} \sin\left(\frac{\alpha_y}{2}\right) - \alpha_y \right] \sqrt{\frac{3\gamma^2 T^2 - \alpha_y^2}{\gamma^2 T^2 + \alpha_y^2}}, \\ v_y &= -\frac{3a}{2T} \left[ \gamma T + 2 \sin\left(\frac{\alpha_y}{2}\right) \right]. \end{aligned} \quad (23)$$

For  $\alpha_y = \sqrt{3}\gamma T$ ,  $v_x$  vanishes. Therefore, we argue that the quasi-energy spectrum would be linear along  $k_y$ . In support of our argument we are going to see the behavior of quasi-energy about the gapless point corresponding to  $\alpha_y = \sqrt{3}\gamma T$ . In this case, we find the gapless point  $(k_x^0, k_y^0) = (0, 4\pi/(9a))$ . Around this point, the quasi-energy spectrum exhibits following semi-Dirac feature:

$$\begin{aligned} \Delta_k^y(k_x^0, k_y) &= \frac{3a\bar{k}_y}{2T} \sqrt{\gamma^2 T^2 + 4 \sin^2\left(\frac{\sqrt{3}\gamma T}{2}\right)}, \\ \Delta_k^y(k_x, k_y^0) &= \frac{\sqrt{3}k_x^2 a^2}{8T} \sqrt{9\gamma^2 T^2 + 4 \sin^2\left(\frac{\sqrt{3}\gamma T}{2}\right)}, \end{aligned} \quad (24)$$

where  $\bar{k}_y = k_y - k_y^0$ . These features are clearly depicted in Fig. 3.

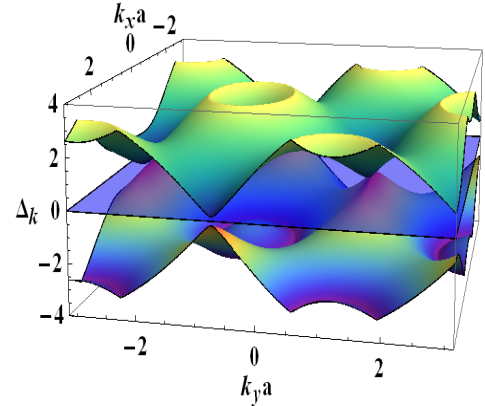


FIG. 3. Sketch of the exact quasi-energy spectrum [Eq.(18)] corresponding to periodic kicking along  $Y$ -direction for  $\alpha_y = \sqrt{3}\gamma T$ . Here, the quasi-energy spectrum exhibits semi-Dirac dispersion around the gapless point  $(0, 4\pi/9a)$  as mentioned in Eq.(24).

### C. Z-Kicking

For the case  $\alpha_z \neq 0$ ,  $\alpha_x = 0$ , and  $\alpha_y = 0$ , the Floquet operator:  $U_F^z(T) = e^{-i\alpha_z S_z} e^{-iH_k T}$  becomes

$$U_F^z(T) = \begin{pmatrix} ae^{-i\alpha_z} & -ib^*e^{-i\alpha_z} & c^*e^{-i\alpha_z} \\ -ib & 2a-1 & -ib^* \\ ce^{i\alpha_z} & -ibe^{i\alpha_z} & ae^{i\alpha_z} \end{pmatrix}, \quad (25)$$

In this case the quasi-energies are obtained as

$$\Delta_k^{z0} = 0, \quad \Delta_k^{z\pm} = \pm\Delta_k^z = \pm\frac{1}{T} \cos^{-1}(\kappa^z), \quad (26)$$

where  $\kappa^z = \cos^2(\alpha_z/2) \cos(\omega_k T) - \sin^2(\alpha_z/2)$ .

Let us check quickly whether gapless points in this particular case still exist or not. If the quasienergy spectrum possesses any gapless point we must have  $\kappa^z = 1$  which implies  $\cos(\omega_k T) = 1 + 2 \tan^2(\alpha_z/2)$ . But this cannot be true because  $\cos(\omega_k T)$  is bounded between  $-1$  and  $1$ . Therefore, the quasienergy spectrum is gapped everywhere. Consider the Dirac points of the unperturbed system where the conduction band touches the valence band. Here,  $\omega_k = 0$ , which consequently implies  $\Delta_k = \alpha_z/T$ . A gap is opened up at the Dirac points. We have  $\Delta_k = \pi/T$  for  $\alpha_z = \pi$ . Therefore, the quasienergy spectrum is independent of the wave vector. This feature is shown in Fig. 4. Similar feature is also obtained in the case of graphene. At  $k$ -values other than the Dirac points i.e.  $\omega_k \neq 0$ , we also have  $\Delta_k = \pi/T$  for  $\alpha_z = \pi$ . This absolutely flat quasienergy bands lead to dynamical localization of wavepacket. On the other hand, for  $\alpha_z = \pi/2$ ,  $\kappa^z = \cos^2(\pi/4) \cos(\omega_k T) - \sin^2(\pi/4)$ . Therefore,  $\Delta_k^{z\pm}$  become dispersive unlike the case for  $\alpha_z = \pi$ . The dispersive and flat quasi-energy bands are depicted in Fig. 4(a) and (b) for  $\alpha_z = \pi/2$  and  $\pi$ , respectively, corroborating the above analytical findings.

### IV. WAVEPACKET DYNAMICS

Having discussed the Floquet quasi-energy dispersion, we now numerically study the time evolution of a wave packet on the dice lattice. Consider an initial Gaussian wave packet  $\Psi$  in two spatial dimensions, with an initial momentum  $k_i = (k_{ix}, k_{iy})$  and a width  $\sigma$  as given below

$$\Psi(\mathbf{r}, t=0) = \frac{1}{\sqrt{2\pi\sigma^2}} \exp\left(-\frac{r^2}{4\sigma^2}\right) \exp(i\mathbf{k}_i \cdot \mathbf{r}), \quad (27)$$

which is normalized such that  $\int d\mathbf{r} |\Psi|^2 = 1$ . We note that the wave packet is centered around  $\mathbf{r} = (0, 0)$  and decaying in  $x$  and  $y$  direction in a uniform (circularly symmetric) manner with localization length  $2\sigma$ . One can consider the Fourier transform of  $\Psi$  to obtain the  $\mathbf{k}$  resolved wave-function

$$\Psi(\mathbf{k}, t=0) = \sqrt{8\pi\sigma^2} \exp[-\sigma^2\{(k_x - k_{ix})^2 + (k_y - k_{iy})^2\}] \quad (28)$$

such that  $\frac{1}{(2\pi)^2} \int dk_x dk_y |\Psi(\mathbf{k})|^2 = 1$ . We use the momentum space wave-function (28) to study the stroboscopic dynamics

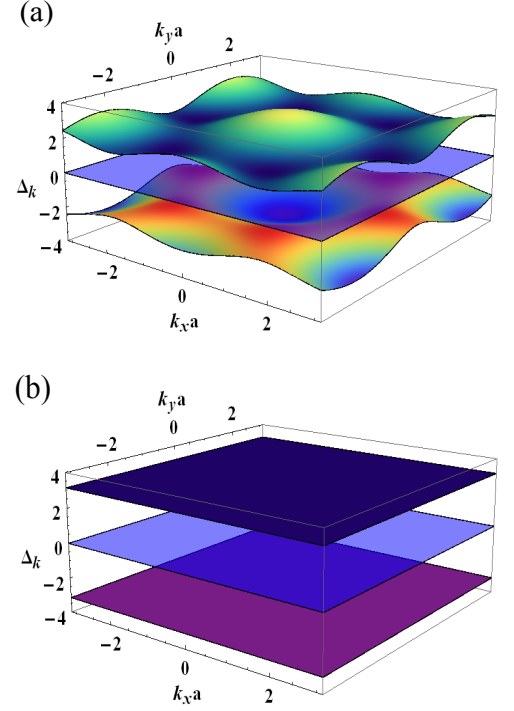


FIG. 4. Sketch of the exact quasi-energy spectrum corresponding to the periodic kicking along the  $Z$ -direction for (a)  $\alpha_z = \pi/2$  and (b)  $\alpha_z = \pi$ . The spectrum is gapped for each value of  $\alpha_z$ . Completely flat quasi-energy bands are obtained for  $\alpha_z = \pi$ .

at integer multiple of  $T$ . Our aim is to understand the subsequent wave packet dynamics from the quasi-energy dispersion  $\Delta_k$ .

The wave packet after  $n$  kicks i.e. at time  $t = nT$  will be obtained by  $n$ -times kick-to-kick operator  $U_F(nT)$  onto  $\Psi(\mathbf{k}, 0)$ . One has to write the initial wave packet in the basis of the dice Hamiltonian (2) as  $\Psi(\mathbf{k}, 0) \rightarrow \Psi(\mathbf{k}, 0)(0, 1, -i)^T/\sqrt{2}$  with  $\mathcal{T}$  being the transpose. We note that the static dice model shows a zero energy flat band and two dispersive valence and conduction bands at finite energies. In the absence of any kicking, the negative energy valence and zero energy flat bands are occupied. We note that the wave packet movement depends on these initially occupied bands. Upon periodic kicking therefore, we have

$$\Psi(\mathbf{k}, t = nT) = U_F(\mathbf{k}, nT)\Psi(\mathbf{k}, 0) = \left[U_F(\mathbf{k}, T)\right]^n \Psi(\mathbf{k}, 0). \quad (29)$$

The driven system continues to preserve the translational symmetry that allows us to study each momentum mode  $\mathbf{k} = (k_x, k_y)$  separately. Thus obtained the  $\mathbf{k}$  resolved wave-function  $\Psi(\mathbf{k}, t = nT)$  is Fourier transformed using the real space lattice structure of dice model. For this, one needs the real space position of each site on the dice lattice  $\mathbf{r} = (x, y)$ . We consider the momentum space Brillouin zone as the rhombus with the vortices  $(\pm 2\pi/\sqrt{3}, 0)$  and  $(0, \pm 2\pi/3)$  and center lying at  $(0, 0)$ . We consider  $N = 40$  blocks of graphene and the total number of lattice sites is  $3N(2N + 1)/2 = 4860$ .

We take periodic boundary condition in real and momentum space to compute the wave packet dynamics.

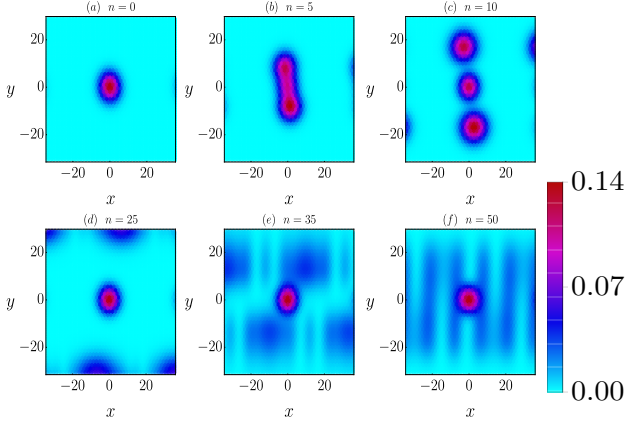


FIG. 5. We show the time evolution of the initial wave-packet centered at  $\mathbf{r} = (0, 0)$  at  $t = 0$  in (a),  $t = 5T$  in (b),  $t = 10T$  in (c),  $t = 25T$  in (d),  $t = 35T$  in (e), and  $t = 50T$  in (f) for  $\alpha_x = \gamma T$ ,  $\alpha_y = \alpha_z = 0$  with  $k_{ix}a = 0.0$  and  $k_{iy}a = 1.0$  and  $\sigma = 5a/\sqrt{2}$ . One can clearly observe that the wave packet evolves with a net velocity along  $y$  direction; however, with time the wave packet spreads in  $x$  direction also. At later time  $t = 50T$  as a result, the localized fringe structure along  $y$  direction is observed. The important point to note here is that there always exists a substantially localized wave-packet centered at  $\mathbf{r} = (0, 0)$  irrespective of the kick as there always exists the flat band in the quasi-energy dispersion.

We first study the wave packet the wave packet dynamics with  $x$  kicking i.e.,  $\alpha_x = \gamma T$ , and  $\alpha_y = \alpha_z = 0$ . We here show that the wave packet spreads along  $y$  direction (see Fig. 5(a,b,c)). This is due to the fact that the initial non-zero momentum is chosen only along  $y$  direction:  $k_{ix}a = 0.0$  and  $k_{iy}a = 1.0$ . With increasing time, fringes like localized structure are formed (see Fig. 5(d,e,f)). The time evolved wave packet thus spreads all over the 2D dice lattice. It is interesting to note that there always exists a wave packet centred around  $\mathbf{r} = (0, 0)$  through out the time evolution. The intermediate energy band continues to remain flat even under the Floquet dynamics as shown in Fig. 2. As a result, the quasi-velocity becomes zero for this band while for the other two finite energy bands, the quasi-velocities become finite and opposite in sign. Since the initial wave packet is projected in these states, we always get the signature of flat band in the centrally localized wave-packet. Due to the finite quasi-velocities of the dispersive bands, the wave packet spreads in both the direction as the initial momentum  $k_{ix}a = 0.0$  and  $k_{iy}a = 1.0$  for wave packet is not located over the dispersionless line with  $k_x = \pi/\sqrt{3}a$ .

We note that  $v_x$  can become finite with  $v_y = 0$  for  $\mathbf{k}_i$  chosen over the dispersionless line causing the initial wave packet to move along  $x$  direction only. At later time, the interfere between different momenta leads to fringe like structure in real space. For  $\alpha_x = 3\gamma T$ , the Floquet quasi-energy dispersion changes leading to a different quasi-velocity as compared to the previous case with  $\alpha_x = \gamma T$ . For small time, wave packet disperses along  $-y$  direction more strongly than  $+y$  direction

(see Fig. 6 (a,b,c)). The wave packet spreading at later times becomes different and fringe pattern gets distorted (see Fig. 6 (d,e,f)). A comparison between Fig. 5 and Fig. 6 clearly suggests that the wave packet movement changes once there exists a gapless line in the quasi-energy dispersion for  $\alpha_x = \gamma T$ . In a similar spirit, we study the wave packet dynamics for  $\alpha_y = \sqrt{3}\gamma T$  as shown in Fig. 7. The wave packet dynamics shows quantitatively different behavior with respect to  $x$  kicking however, qualitatively  $x$  and  $y$  kicking result in similar behavior. The delocalization of the Gaussian wave packet is observed.

We shall now analyze the  $z$  kicking as shown in Fig. 8 and Fig. 9 for  $\alpha_z = \pi/2$  and  $\alpha_z = \pi$ , respectively. The stark distinction can be noticed for the later case where dynamical localization is clearly observed. The initial Gaussian wave packet, centred around  $\mathbf{r} = (0, 0)$ , is frozen with time. This can be explained by the fact that all the Floquet quasi-bands becomes flat as shown in Fig. 4. The quasi-velocity vanishes for all the bands identically leading to the dynamically localized wave packet. On the other hand, with  $\alpha_z = \pi/2$ , the initial Gaussian wave packet does not get delocalized for small times rather it the wave packet moves as a whole along  $-y$  direction (see 8 (a,b,c)). At later time, finite quasi velocity causes the wave packet to spread over the real space lattice (see 8 (d,e,f)). This can be explained from the fact that gapped quasi-energy (see 4 (a)) spectrum is actually dispersive in nature.

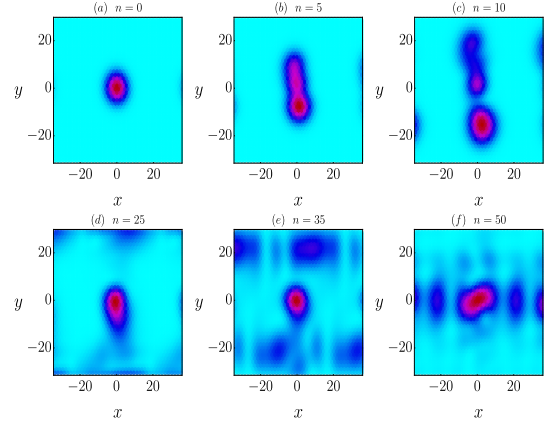


FIG. 6. We repeat Fig. 5 with  $\alpha_x = 3\gamma T$ . The wave packet moves along  $y$  direction, however, the weight transfer in a non-uniform manner. The wave packet moving in the  $-y$  direction shows higher degree of localization as compared to the wave packet moving in  $+y$  direction. At later time, the localized fringe structure along  $y$  direction, as observed for Fig. 5, becomes distorted. The localized structure of wave packet at  $\mathbf{r} = (0, 0)$  remains unaltered as the flat band continues to exist in the dynamics.

## V. CONCLUSION

In conclusion, we study the stroboscopic properties of a time-periodic  $\delta$ -kicked dice lattice which has pseudospin-1. We find that with the help of the  $\delta$ -kicking, a variety of low

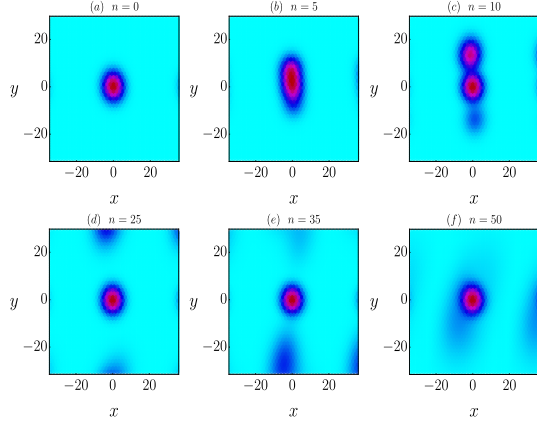


FIG. 7. We repeat Fig. 5 with  $\alpha_y = \sqrt{3}\gamma T$ , and  $\alpha_x = \alpha_z = 0$ . The wave packet moves substantially along  $+y$  direction. At later time, the fringe like structure of localized wave packet is not observed unlike the  $x$ -kicking. The flat band continues to persist as the centrally localized wave packet remain there with time.

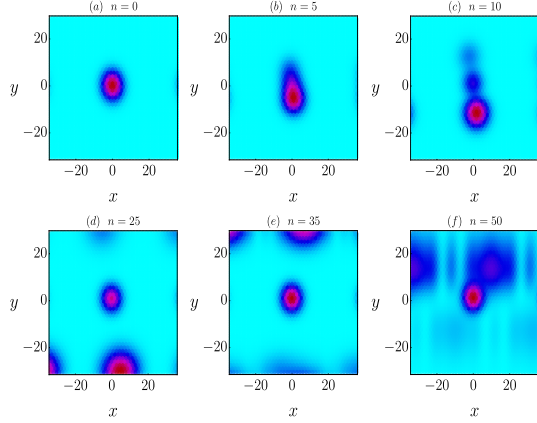


FIG. 8. We repeat Fig. 5 with  $\alpha_z = \pi/2$ , and  $\alpha_x = \alpha_y = 0$ . For small time, the wave packet as a whole moves along  $-y$  direction. At later time, the localized fringe structure arises in addition to the centrally localized wave packet.

energy dispersions including semi-Dirac type, gapless line,

absolute flat quasi-energy bands can be engineered around some specific points in the Brillouin zone. The underlying static model does not support these various types of dispersion. Therefore, our study can motivate the non-equilibrium transport studies on dice model given the fact that various quasi-energy dispersion can lead to interesting transport behavior. In order to visualize the different aspects of quasi-energy dispersion, we investigate the wave packet dynamics as a function of stroboscopic time. The study of wave packet dynamics reveals the existence of dynamical localization of electronic wavepacket for a periodic kicking in the transverse direction. The dynamical localization is caused by the flat quasi-energy bands. In the context of topological system, dice model could be an important candidate due to its zero energy flat band.

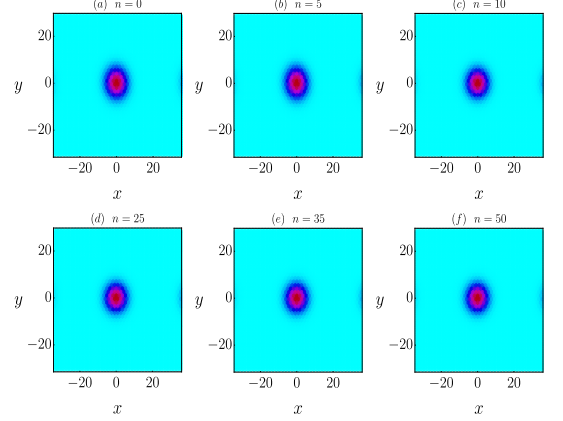


FIG. 9. We repeat Fig. 8 with  $\alpha_z = \pi$ . Here, we clearly observe the dynamical localization as the initial wave packet remains frozen at its localization core. This situation is corroborated with the fact that all three quasi-bands become flat and hence the quasi-velocity vanishes identically for all these bands. This is in stark contrast to all of the previous situation where initial wave packet disperses with time.

## VI. ACKNOWLEDGEMENT

One of the authors (L. T.) sincerely acknowledges the financial supports provided by University of North Bengal through University Research Projects to pursue this work.

## Appendix A

Here, we provide a derivation of the Floquet quasi-energy spectrum in detail. The calculations for  $X$  and  $Y$  kicking are similar and that for the  $Z$ -kicking is less cumbersome. So, we derive quasi-energy spectrum corresponding to  $X$ -kicking only in a straightforward manner.

The Floquet operator for  $X$ -kicking is reduced to  $U_F^x(T) = e^{-i\alpha_x S_x} e^{-iH_k T}$ . We need to find out the eigenvalues of  $U_F^x(T)$  in a straightforward manner in order to calculate the corresponding quasi-energy  $\Delta_k$ .

With the following general formula of a  $3 \times 3$  rotation matrix

$$U_\mu(\phi) \equiv \exp(iS_\mu\phi) = \mathbf{1} - i \sin \phi S_\mu - (1 - \cos \phi) S_\mu^2 \quad (\text{A1})$$



with  $\mu = x, y, z$ , we find

$$\exp(-i\alpha_x S_x) = \begin{pmatrix} \frac{1}{2}(1 + \cos \alpha_x) & -\frac{i}{\sqrt{2}} \sin \alpha_x & \frac{1}{2}(-1 + \cos \alpha_x) \\ -\frac{i}{\sqrt{2}} \sin \alpha_x & \cos \alpha_x & -\frac{i}{\sqrt{2}} \sin \alpha_x \\ \frac{1}{2}(-1 + \cos \alpha_x) & -\frac{i}{\sqrt{2}} \sin \alpha_x & \frac{1}{2}(1 + \cos \alpha_x) \end{pmatrix} = \begin{pmatrix} p & -iq & r \\ -iq & 2p-1 & -iq \\ r & -iq & p \end{pmatrix}, \quad (\text{A2})$$

where  $p = (1 + \cos \alpha_x)/2$ ,  $q = \sin \alpha_x/\sqrt{2}$ , and  $r = (-1 + \cos \alpha_x)/2$ .

We further find

$$\exp(-iH_{\mathbf{k}}T) = \begin{pmatrix} \frac{1}{2}[1 + \cos(\omega_{\mathbf{k}}T)] & -\frac{i}{\sqrt{2}}e^{i\theta_{\mathbf{k}}} \sin(\omega_{\mathbf{k}}T) & \frac{1}{2}e^{2i\theta_{\mathbf{k}}}[-1 + \cos(\omega_{\mathbf{k}}T)] \\ -\frac{i}{\sqrt{2}}e^{-i\theta_{\mathbf{k}}} \sin(\omega_{\mathbf{k}}T) & \cos(\omega_{\mathbf{k}}T) & -\frac{i}{\sqrt{2}}e^{i\theta_{\mathbf{k}}} \sin(\omega_{\mathbf{k}}T) \\ \frac{1}{2}e^{-2i\theta_{\mathbf{k}}}[-1 + \cos(\omega_{\mathbf{k}}T)] & -\frac{i}{\sqrt{2}}e^{-i\theta_{\mathbf{k}}} \sin(\omega_{\mathbf{k}}T) & \frac{1}{2}e^{-2i\theta_{\mathbf{k}}}[1 + \cos(\omega_{\mathbf{k}}T)] \end{pmatrix} = \begin{pmatrix} a & -ib^* & c^* \\ -ib & 2a-1 & -ib^* \\ c & -ib & a \end{pmatrix} \quad (\text{A3})$$

where  $a = [1 + \cos(\omega_{\mathbf{k}}T)]/2$ ,  $b = e^{-i\theta_{\mathbf{k}}} \sin(\omega_{\mathbf{k}}T)/\sqrt{2}$ , and  $c = e^{-2i\theta_{\mathbf{k}}}[1 + \cos(\omega_{\mathbf{k}}T)]/2$ . Note that  $f_{\mathbf{k}} = \omega_{\mathbf{k}}e^{i\theta_{\mathbf{k}}}$ .

Now the Floquet operator can be written as

$$U_F^x(T) = \begin{pmatrix} A & -iB^* & C^* \\ -iP & Q & -iP^* \\ C & -iB & A^* \end{pmatrix}, \quad (\text{A4})$$

where

$$\begin{aligned} A &= pa - qb + rc \\ B &= pb + q(2a - 1) + rb^* \\ C &= pc - qb + ra \\ P &= (2p - 1)b + q(a + c) \\ Q &= (2p - 1)(2a - 1) - q(b + b^*). \end{aligned}$$

We will find the eigen values of  $U_F^x(T)$  in a straightforward way. The characteristic equation is

$$\begin{vmatrix} A - \lambda & -iB^* & C^* \\ -iP & Q - \lambda & -iP^* \\ C & -iB & A^* - \lambda \end{vmatrix} = 0. \quad (\text{A5})$$

Expanding this we will find the following cubic equation

$$\lambda^3 - (A + A^* + Q)\lambda^2 + \left[ (A + A^*)Q + |A|^2 - |C|^2 + 2\text{Re}(BP^*) \right] \lambda - \left[ (|A|^2 - |C|^2)Q + 2\text{Re}\{B(AP^* - PC^*)\} \right] = 0 \quad (\text{A6})$$

It is straightforward to show the coefficients of  $\lambda$  and  $\lambda^2$  are equal and the last term will be equal to 1.

Therefore, we have

$$\lambda^3 - (A + A^* + Q)\lambda^2 + (A + A^* + Q)\lambda - 1 = 0, \quad (\text{A7})$$

which further gives  $\lambda = 1$  and

$$\lambda^2 - 2\kappa^x \lambda + 1 = 0, \quad (\text{A8})$$

where  $2\kappa^x = A + A^* + Q - 1$ .

Therefore, we find

$$\lambda_{\pm} = \kappa^x \pm \sqrt{(\kappa^x)^2 - 1}. \quad (\text{A9})$$

Note that

$$\kappa^x = \frac{1}{2}(\cos \alpha_x - 1) \sin^2 \theta_{\mathbf{k}} - \sin \alpha_x \cos \theta_{\mathbf{k}} \sin(\omega_{\mathbf{k}}T) + \frac{1}{2}[\sin^2 \theta_{\mathbf{k}} + \cos \alpha_x(1 + \cos^2 \theta_{\mathbf{k}})] \cos(\omega_{\mathbf{k}}T) \quad (\text{A10})$$

and consequently  $(\kappa^x)^2 < 1$ .

Therefore we have

$$\lambda_{\pm} = \kappa^x \pm i\sqrt{1 - (\kappa^x)^2}. \quad (\text{A11})$$

We can now set  $\lambda_{\pm} = e^{\pm i\Delta_{\mathbf{k}}^x T}$ . Therefore the corresponding quasienergies are obtained as

$$\Delta_{\mathbf{k}}^{x\pm} = \pm \frac{1}{T} \cos^{-1}(\kappa^x). \quad (\text{A12})$$

Final result is

$$\Delta_{\mathbf{k}}^{x0} = 0, \quad \Delta_{\mathbf{k}}^{x\pm} = \pm \frac{1}{T} \cos^{-1}(\kappa^x). \quad (\text{A13})$$

---

\* [tnag@physik.rwth-aachen.de](mailto:tnag@physik.rwth-aachen.de)

† [tbiswas@nbu.ac.in](mailto:tbiswas@nbu.ac.in)

- <sup>1</sup> K. S. Novoselov, A. K. Geim, S. V. Morozov, D. Jiang, Y. Zhang, S. V. Dubonos, I. V. Grigorieva, and A. A. Firsov, *Science* **306**, 666 (2004).
- <sup>2</sup> A. H. Castro Neto, F. Guinea, N. M. R. Peres, K. S. Novoselov, and A. K. Geim, *Rev. Mod. Phys.* **81**, 109 (2009).
- <sup>3</sup> S. Das Sarma, S. Adam, E. H. Hwang, and E. Rossi, *Rev. Mod. Phys.* **83**, 407 (2011).
- <sup>4</sup> M. O. Goerbig, *Rev. Mod. Phys.* **83**, 1193 (2011).
- <sup>5</sup> F. Schwierz, *Nature Nanotechnology* **5**, 487 (2010).
- <sup>6</sup> B. Sutherland, *Phys. Rev. B* **34**, 5208 (1986).
- <sup>7</sup> J. Vidal, R. Mosseri, and B. Doucot, *Phys. Rev. Lett.* **81**, 5888 (1998).
- <sup>8</sup> F. Wang and Y. Ran, *Phys. Rev. B* **84**, 241103 (2011).
- <sup>9</sup> D. Bercioux, D. F. Urban, H. Grabert, and W. Häusler, *Phys. Rev. A* **80**, 063603 (2009).
- <sup>10</sup> A. Raoux, M. Morigi, J.-N. Fuchs, F. Piechon, and G. Montambaux, *Phys. Rev. Lett.* **112**, 026402 (2014).
- <sup>11</sup> S. E. Korshunov, *Phys. Rev. B* **63**, 134503 (2001).
- <sup>12</sup> M. Rizzi, V. Cataudella, and R. Fazio, *Phys. Rev. B* **73**, 144511 (2006).
- <sup>13</sup> D. Bercioux, M. Governale, V. Cataudella, and V. M. Ramaglia, *Phys. Rev. Lett.* **93**, 056802 (2004); *Phys. Rev. B* **72**, 075305 (2005).
- <sup>14</sup> D. F. Urban, D. Bercioux, M. Wimmer, and W. Häusler, *Phys. Rev. B* **84**, 115136 (2011).
- <sup>15</sup> E. Illes and E. J. Nicol, *Phys. Rev. B* **95**, 235432 (2017).
- <sup>16</sup> J. D. Malcolm and E. J. Nicol, *Phys. Rev. B* **93**, 165433 (2016).
- <sup>17</sup> A. Balassis, D. Dahal, G. Gumbs, A. Iurov, D. Huang and O. Roslyak, *J. Phys.: Condens. Matter* **32**, 485301 (2020).
- <sup>18</sup> E. Illes, J. P. Carbotte, and E. J. Nicol, *Phys. Rev. B* **92**, 245410 (2015).
- <sup>19</sup> E. Illes, and E. J. Nicol, *Phys. Rev. B* **94**, 125435 (2016).
- <sup>20</sup> A. D. Kovacs, G. David, B. Dora, and J. Cserti, *Phys. Rev. B* **95**, 035414 (2017).
- <sup>21</sup> T. Biswas and T. K. Ghosh, *J. Phys.: Condens. Matter* **28**, 495302 (2016).
- <sup>22</sup> SKF Islam, *P Dutta Physical Review B* **96**, 045418 (2017).
- <sup>23</sup> T. Biswas and T. K. Ghosh, *J. Phys.: Condens. Matter* **30**, 075301 (2018).
- <sup>24</sup> L. Chen, J. Zuber, Z. Ma, and C. Zhang, *Phys. Rev. B* **100**, 035440 (2019).
- <sup>25</sup> D. O. Oriekhov and V. P. Gusynin, *Phys. Rev. B* **101**, 235162 (2020).
- <sup>26</sup> O. Roslyak, G. Gumbs, A. Balassis, H. Elsayed, *arXiv:2006.15447v2*.
- <sup>27</sup> J. Wang, J. F. Liu and C. S. Ting *Phys. Rev. B* **101**, 205420 (2020).
- <sup>28</sup> B. Dey, P. Kapri, O. Pal, T. K. Ghosh, *Phys. Rev. B* **101**, 235406 (2020).
- <sup>29</sup> J. W. McClure, *Phys. Rev.* **104**, 666 (1956).
- <sup>30</sup> G. Floquet, *Annales de l'Ecole Normale Supérieure* **12**, 47 (1883).
- <sup>31</sup> J. H. Shirley, *Phys. Rev.* **138**, B979 (1965).
- <sup>32</sup> T. Oka and H. Aoki, *Phys. Rev. B* **79**, 081406 (2009).
- <sup>33</sup> T. Kitagawa, T. Oka, A. Brataas, L. Fu, and E. Demler, *Phys. Rev. B* **84**, 235108 (2011).
- <sup>34</sup> Z. Gu, H. A. Fertig, D. P. Arovas, and A. Auerbach, *Phys. Rev. Lett.* **107**, 216601 (2011).
- <sup>35</sup> E. Suarez Morell and L. E. F. Foa Torres, *Phys. Rev. B* **86**, 125449 (2012).
- <sup>36</sup> N. H. Lindner, G. Refael, and V. Galitski, *Nat. Phys.* **7**, 490 (2011).
- <sup>37</sup> J. Cayssol, B. Dóra, F. Simon, and R. Moessner, *Phys. Status Solidi RRL* **7**, 101 (2013).
- <sup>38</sup> M. S. Rudner and N. H. Lindner, *Nature Reviews Physics* **2**, 229 (2020).
- <sup>39</sup> A. G. Grushin, A. Gomez-Leon, and T. Neupert, *Phys. Rev. Lett.* **112**, 156801 (2014).
- <sup>40</sup> J. Klinovaja, P. Stano, and D. Loss, *Phys. Rev. Lett.* **116**, 176401 (2016).
- <sup>41</sup> J. Liu, K. Hejazi, and L. Balents, *Phys. Rev. Lett.* **121**, 107201 (2018).
- <sup>42</sup> F. Gorg, M. Messer, K. Sandholzer, G. Jotzu, R. Desbuquois, and T. Esslinger, *Nature* **553**, 481 (2018).
- <sup>43</sup> D. M. Kennes, A. de la Torre, A. Ron, D. Hsieh, and A. J. Millis, *Phys. Rev. Lett.* **120**, 127601 (2018).
- <sup>44</sup> F. Harper, R. Roy, M. S. Rudner, and S. L. Sondhi, *arXiv:1905.01317* (2019).
- <sup>45</sup> C. W. von Keyserlingk and S. L. Sondhi, *Phys. Rev. B* **93**, 245145 (2016).
- <sup>46</sup> A. C. Potter, T. Morimoto, and A. Vishwanath, *Phys. Rev. X* **6**, 041001 (2016).
- <sup>47</sup> D. V. Else and C. Nayak, *Phys. Rev. B* **93**, 201103 (2016).
- <sup>48</sup> F. Harper and R. Roy, *Phys. Rev. Lett.* **118**, 115301 (2017).
- <sup>49</sup> T. Kitagawa, E. Berg, M. Rudner, and E. Demler, *Phys. Rev. B* **82**, 235114 (2010).
- <sup>50</sup> M. S. Rudner, N. H. Lindner, E. Berg, and Michael Levin, *Phys. Rev. X* **3**, 031005 (2013).
- <sup>51</sup> F. Nathan and M. S. Rudner, *New J. Phys.* **17**, 125014 (2015).
- <sup>52</sup> R. Roy and F. Harper, *Phys. Rev. B* **95**, 195128 (2017).
- <sup>53</sup> R. Roy and F. Harper, *Phys. Rev. B* **96**, 155118 (2017).
- <sup>54</sup> S. Yao, Z. Yan, and Z. Wang, *Phys. Rev. B* **96**, 195303 (2017).
- <sup>55</sup> A. Gomez-Leon and G. Platero, *Phys. Rev. Lett.* **110**, 200403 (2013).
- <sup>56</sup> G. M. Graf and C. Tauber, *Ann. Henri Poincaré* **19**, 709 (2018).
- <sup>57</sup> J. Shapiro and C. Tauber, *Annales Henri Poincaré* **20**, 1837 (2019).

- (2019).
- <sup>58</sup> V. Khemani, A. Lazarides, R. Moessner, and S. L. Sondhi, *Phys. Rev. Lett.* **116**, 250401 (2016).
  - <sup>59</sup> D. V. Else, B. Bauer, and C. Nayak, *Phys. Rev. Lett.* **117**, 090402 (2016).
  - <sup>60</sup> D. V. Else, B. Bauer, and C. Nayak, *Phys. Rev. X* **7**, 011026 (2017).
  - <sup>61</sup> M. S. Rudner and J. C. W. Song, *Nature Physics* (2019).
  - <sup>62</sup> T. Nag, R. Slager, T. Higuchi, and T. Oka, *Phys. Rev. B* **100**, 134301 (2019).
  - <sup>63</sup> S. Kinoshita, K. Murata, and T. Oka, *Journal of High Energy Physics* **96**, 2018 (2018).
  - <sup>64</sup> F. Harper, R. Roy, M. S. Rudner, and S. L. Sondhi, *arXiv:1905.01317* (2019).
  - <sup>65</sup> B. Dey and T. K. Ghosh, *Phys. Rev. B* **98**, 075422 (2018).
  - <sup>66</sup> M. Trif and Y. Tserkovnyak, *Phys. Rev. Lett.* **109**, 257002 (2012).
  - <sup>67</sup> D. E. Liu, A. Levchenko, and H. U. Baranger, *Phys. Rev. Lett.* **111**, 047002 (2013).
  - <sup>68</sup> Q.-J. Tong, J.-H. An, J. Gong, H.-G. Luo, and C. H. Oh, *Phys. Rev. B* **87**, 201109(R) (2013).
  - <sup>69</sup> A. Kundu and B. Seradjeh, *Phys. Rev. Lett.* **111**, 136402 (2013).
  - <sup>70</sup> A. A. Reynoso and D. Frustaglia, *Phys. Rev. B* **87**, 115420 (2013).
  - <sup>71</sup> A. Ghosh, T. Nag and A. Saha, *arXiv:2009.11220*.
  - <sup>72</sup> M. S. Rudner, N. H. Lindner, E. Berg, and M. Levin, *Phys. Rev. X* **3**, 031005 (2013).
  - <sup>73</sup> P. M. Perez-Piskunow, G. Usaj, C. A. Balseiro, and L. E. F. Foa Torres, *Phys. Rev. B* **89**, 121401(R) (2014).
  - <sup>74</sup> G. Usaj, P. M. Perez-Piskunow, L. E. F. Foa Torres, and C. A. Balseiro, *Phys. Rev. B* **90**, 115423 (2014).
  - <sup>75</sup> P. M. Perez-Piskunow, L. E. F. Foa Torres, and G. Usaj, *Phys. Rev. A* **91**, 043625 (2015).
  - <sup>76</sup> M. D. Reichl and E. J. Mueller, *Phys. Rev. A* **89**, 063628 (2014).
  - <sup>77</sup> P. Delplace, A. Gómez-León, and G. Platero, *Phys. Rev. B* **88**, 245422 (2013).
  - <sup>78</sup> B. Dey and T. K. Ghosh, *Phys. Rev. B* **99**, 205429 (2019).
  - <sup>79</sup> T. Nag, A. Rajak, *arXiv:2001.01378*.
  - <sup>80</sup> G. Jotzu, M. Messer, R. Desbuquois, M. Lebrat, T. Uehlinger, D. Greif, and T. Esslinger, *Nature* **515**, 237 (2014).
  - <sup>81</sup> N. Flaschner, B. S. Rem, M. Tarnowski, D. Vogel, D.- S. Luhmann, K. Sengstock, and C. Weitenberg, *Science* **352**, 1091 (2016).
  - <sup>82</sup> M. C. Rechtsman, J. M. Zeuner, Y. Plotnik, Y. Lumer, D. Podolsky, F. Dreisow, S. Nolte, M. Segev, and A. Szameit, *Nature* **496**, 196 (2013).
  - <sup>83</sup> Y. H. Wang, H. Steinberg, P. Jarillo-Herrero, and N. Gedik, *Science* **342**, 453 (2013).
  - <sup>84</sup> J. W. McIver, B. Schulte, F.-U. Stein, T. Matsuyama, G. Jotzu, G. Meier, and A. Cavalleri, *Nature Physics* **16**, 38 (2020).
  - <sup>85</sup> S. Dasgupta, U. Bhattacharya, and A. Dutta, *Phys. Rev. E* **91**, 052129 (2015).
  - <sup>86</sup> T. Nag, S. Roy, A. Dutta, and D. Sen, *Phys. Rev. B* **89**, 165425 (2014).
  - <sup>87</sup> R. W. Bomantara, G. N. Raghava, L. Zhou, and J. Gong, *Phys. Rev. E* **93**, 022209 (2016).
  - <sup>88</sup> M. Lababidi, I. I. Satija, and E. Zhao, *Phys. Rev. Lett.* **112**, 026805 (2014).
  - <sup>89</sup> A. Agarwala, U. Bhattacharya, A. Dutta, and D. Sen, *Phys. Rev. B* **93**, 174301 (2016).
  - <sup>90</sup> M. Thakurathi, A. A. Patel, D. Sen, and A. Dutta, *Phys. Rev. B* **88**, 155133 (2013).
  - <sup>91</sup> M. Thakurathi, K. Sengupta, and D. Sen, *Phys. Rev. B* **89**, 235434 (2014).
  - <sup>92</sup> L. C. Wang, X. P. Li, and C. F. Li, *Phys. Rev. B* **95**, 104308 (2017).
  - <sup>93</sup> T. Mishra, A. Pallaprolu, T. Guha Sarkar, and J. N. Bandyopadhyay, *Phys. Rev. B* **97**, 085405 (2018).
  - <sup>94</sup> T. Nag, V. Juricic, B. Roy, *Phys. Rev. Research* **1**, 032045(R) (2019), T. Nag, V. Juricic, B. Roy, *arXiv:2009.10719*.
  - <sup>95</sup> B. V. Chirikov, F. M. Izrailev, and D. L. Shepelyansky, *Sov. Sci. Rev. C* **2**, 209 (1981).
  - <sup>96</sup> S. Fishman, D. R. Grempel, and R. E. Prange, *Phys. Rev. Lett.* **49**, 509 (1982).
  - <sup>97</sup> H. Ammann, R. Gray, I. Shvarchuck, and N. Christensen, *Phys. Rev. Lett.* **80**, 4111 (1998).
  - <sup>98</sup> F. Grossmann, T. Dittrich, P. Jung, and P. Hänggi, *Phys. Rev. Lett.* **67**, 516 (1991).
  - <sup>99</sup> P. L. Kapitza, *Sov. Phys. JETP* **21**, 588 (1951).
  - <sup>100</sup> H. W. Broer, I. Hoveijn, M. van Noort, C. Simon, and G. Vegter, *Journal of Dynamics and Differential Equations*, **16**, 897 (2004).
  - <sup>101</sup> B. Horstmann, J. I. Cirac, and T. Roscilde, *Phys. Rev. A* **76**, 043625 (2007).